Bioorganic & Medicinal Chemistry Letters 20 (2010) 1–25

Contents lists available at ScienceDirect

Bioorganic & Medicinal Chemistry Letters

journal homepage: www.elsevier.com/locate/bmcl

Bioorganic & Medicinal Chemistry Letters Volume 20, Issue 1, 2010

Contents

ARTICLES

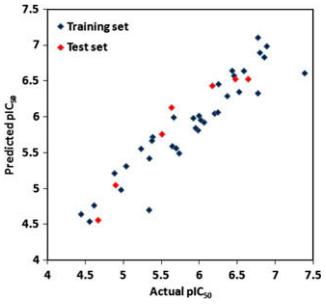

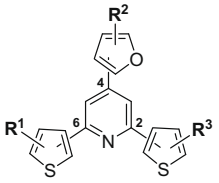

R^1, **R**^{2}, **R**^{3}: -H, -CH_3 or -Cl

For the development of novel antitumor agents, 2,6-dithienyl-4-furyl pyridine derivatives were prepared and evaluated for their topoisomerase I and II inhibitory activity as well as cytotoxicity against several human cancer cell lines.

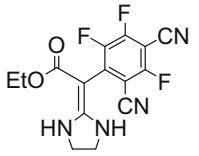

5o IC_{50} = 0.02 μ *g*/mL

A series of polyhalo heterocyclic ketene aminals (HKAs) were synthesized under solvent-free conditions and evaluated in vitro against a panel of human tumor cell lines. Trifluoro-HKAs were the most cytotoxic compounds, then difluoro-HKAs and trichloro-HKAs. Ethoxycarbonyl substituted **5o** was found to be the most potent derivative with IC_{50} values lower than 3.7 μg/mL against 5 human tumor cell lines making it more active than cisplatin (DDP).

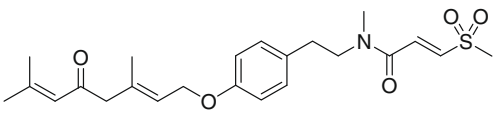

Methylgerambullone (MGB, **1**)

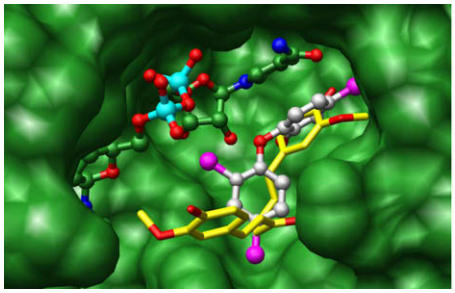

Curcumin has been proved to be an uncompetitive inhibitor of enoyl-ACP reductase from *Escherichia coli* (*Ec*FabI) with the inhibition constant (K_i) of 15 μM. Particularly, curcumin had apparent antibacterial activity against *E. coli*, and the corresponding MIC_{90} was 73.7 μg/mL.

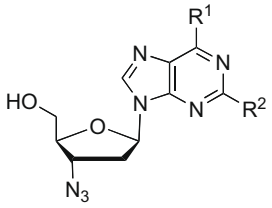

A series of purine modified 3′-azido nucleosides were synthesized by a chemical transglycosylation reaction and evaluated for their anti-HIV-1 activity, cytotoxicity and intracellular metabolism.

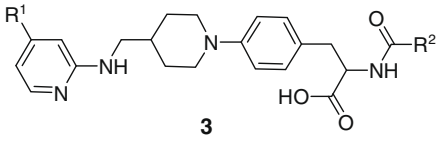

3

Correlation of structural features of selected *N*-phenyl piperidine derivatives **3** with integrin α5β1 binding affinities and selectivities as well as pharmacokinetic properties are described. The best compounds were compared in pharmacokinetic studies in rat.

A multiple linear regression QSAR model was developed based on a set of 61 compounds with internally consistent permeability data measured across Franz cell. The data was normalized using a mean permeability value of a reference compound, 3-isobutyl-1-methylxanthine (IBMX). The QSAR model contained only five simple descriptors and had a correlation coefficient, r^2 of 0.77 between experimental and calculated values for skin permeability. The mean absolute error was 0.3 for the entire set and the cross validation coefficient, q^2 was 0.71. The in silico skin permeability model was used as a filter for virtual libraries and to optimize skin permeation of specific compounds for several dermatology discovery projects. logPe=6.6177-0.0022*PISA-0.3516*donorHB-0.2451*acceptHB-5.8373*glob+0.2700*EA(eV)

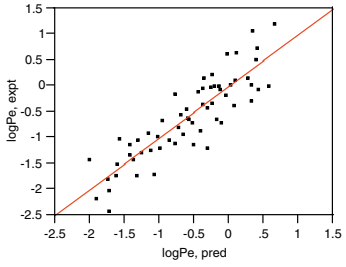

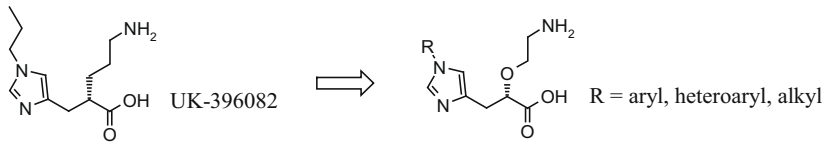

Oxygenated side-chain analogues of clinical candidate UK-396082 were found to be potent inhibitors of activated thrombin activatable fibrinolysis inhibitor (TAFIa).

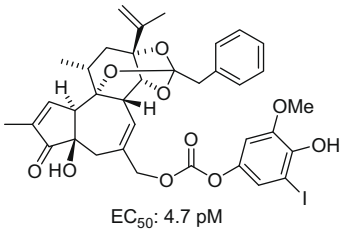

EC_{50}: 4.7 pM

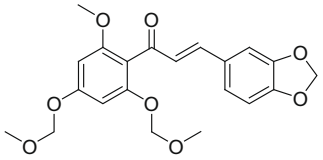

42, 92% Reduction of parasite burden after 4 weeks

The in vitro screening of 43 polysubstituted chalcones against *Leishmania amazonensis* axenic amastigotes, lead to the evaluation of nine of them in a macrophage-infected model with the two other most infectious *Leishmania* species prevalent in Peru (*Leishmania braziliensis* and *Leishmania peruviana*), five of the most active and selective were studied in vivo, resulting on the identification of two chalcones with high reduction parasite burden percentages.

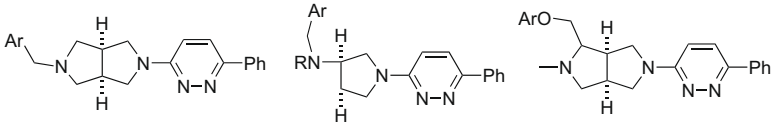

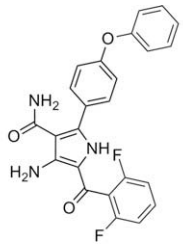

22
Lck IC_{50} = 1.3 nM, MLR IC_{50} =31 nM

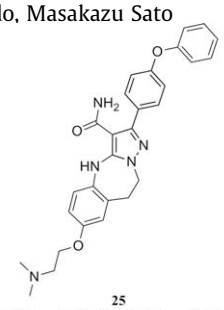

25
Lck IC_{50} = 0.72 nM, MLR IC_{50} = 0.74 nM

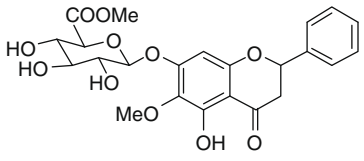

1

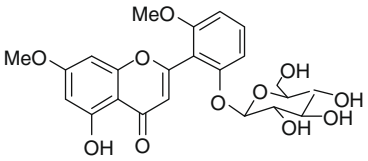

2

Phytochemical investigation of the stem bark of the *O.indicum* yielded two new compounds (**1**, **2**) along with known compounds (**3–9**). Antiulcer activity of the isolates was studied on various models.

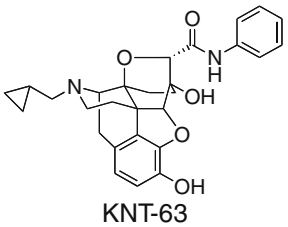

KNT-63

KNT-63 designed on the basis of an active conformation of selective κ agonist TRK-820 showed strong antinociceptive effects via the κ receptor.

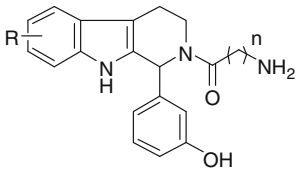

A series of tetrahydro-β-carbolines were identified by HTS as inhibitors of the kinesin Eg5. Molecular modeling and medicinal chemistry techniques were employed to explore the SAR for this series with a focus of removing potential metabolic liabilities and improving cellular potency.

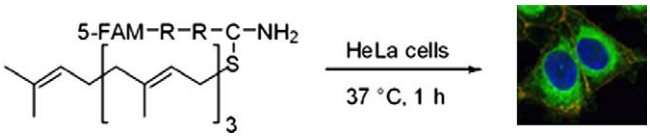

Laterocidin and its analogues **1–6** were synthesized by solid-phase techniques with side chain carboxyl group of Aspartate linked to Rink resin by using Dmab group as a temporary α-COOH protecting group during solid-phase synthesis with Fmoc chemistry. Laterocidin analogue **3** exhibits potent and broad antibacterial activities.

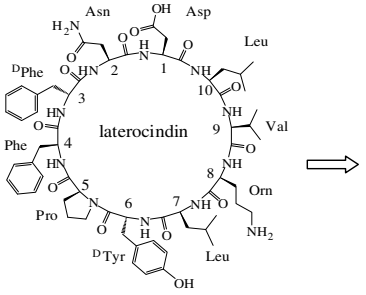

laterocidin: cyclo[-LVOL(^{D}Y)PF(^{D}F)ND-]
1. cyclo[-LVOL(^{D}Y)PF(^{D}F)NN-]
2. cyclo[-LVOL(^{D}F)PF(^{D}F)NN-]
3. cyclo[-LVOL(^{D}F)PY(^{D}F)NN-]
4. cyclo[-LVOL(^{D}F)PYFNN-]
5. cyclo[-LVOLFPY(^{D}F)NN-]
6. cyclo[-LVOLFPYFNN-]

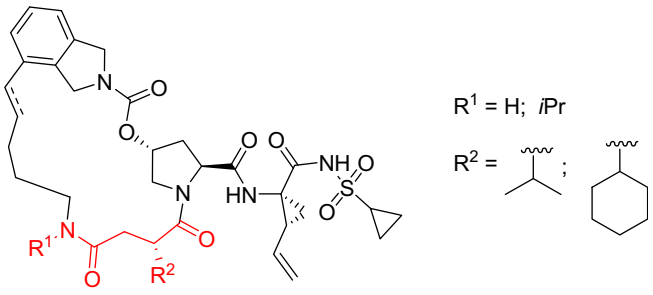

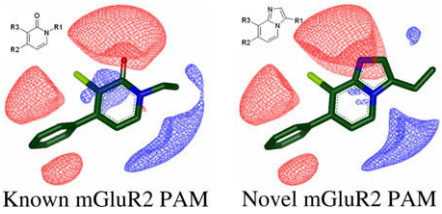

Shape and electrostatic virtual screening identified the imidazopyridine as highly similar to the pyridone mGluR2 PAM scaffold. Example compounds were synthesized and show good primary activity and promise for future work.

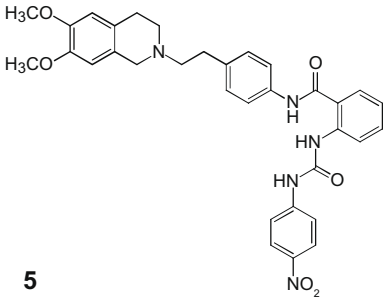

5

Compound **5** is a novel lead for the design of new and potent BCRP modulators.

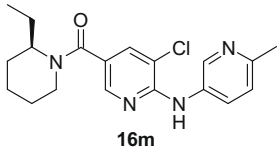

16m

Novel mGluR5 antagonists have been developed. SAR studies and lead optimizations are described, which result in compound **16m** with high efficacy in animal models.

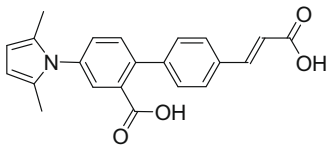

GLS_22 EC_{50} = 4.9 μM

A new series of *N*-carboxyphenylpyrrole ligands were designed using GeometryFit based on an X-ray crystal structure of gp41. The synthesized ligands showed significant inhibitory activities against HIV gp41 6-helix bundle formation, HIV-1 mediated cell-cell fusion and HIV-1 replication.

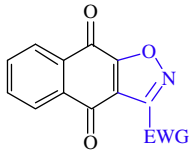

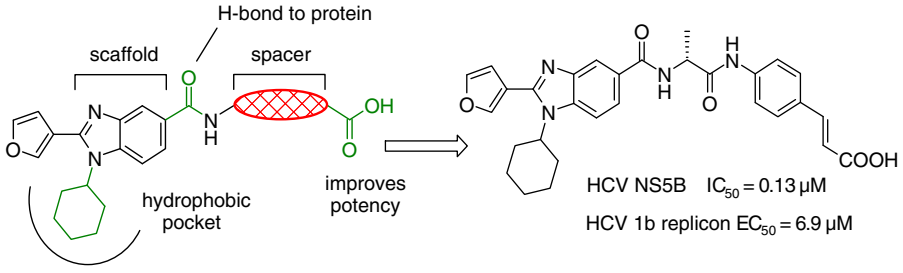

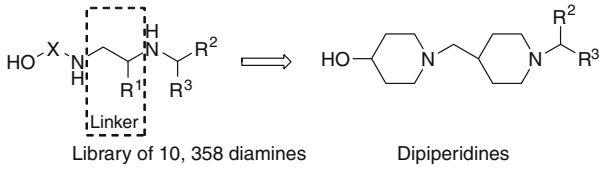

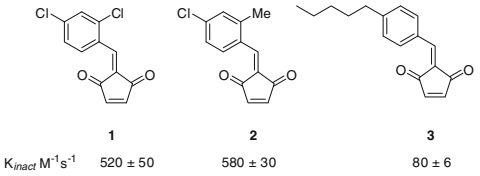

A series of benzylidene cyclopentenedione-based inhibitors, acting through covalent modification of the active site of botulinum neurotoxin A light chain metalloprotease, are reported.

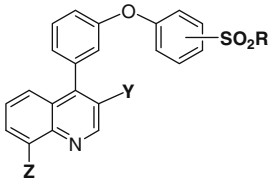

7 R = alkyl
Y = CH_2Ph, Me, H
Z = Cl, CF_3

A series of 4-(3-aryloxyaryl)quinoline sulfones **7** was prepared as LXR agonists.

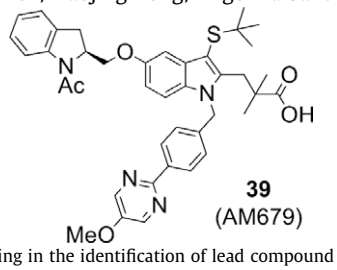

39 (AM679)

The SAR of a potent series of FLAP inhibitors is described culminating in the identification of lead compound **39** (AM679).

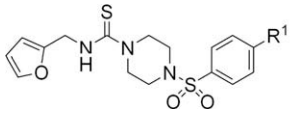

1a $R^1 = NO_2$
1b R^1 = Cl

The synthesis and antiplasmodial activity of analogs based on piperazine sulfonamides screening positives **1a**–**b** is reported.

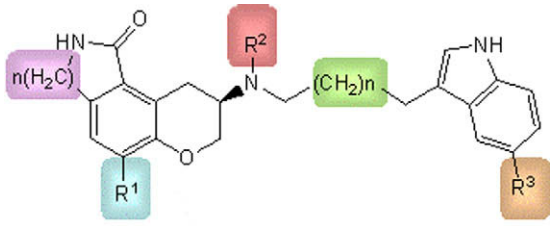

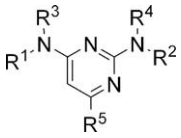

The synthesis, antiplasmodial activity and selected DMPK properties of novel 2,4-diaminopyrimidines is reported.

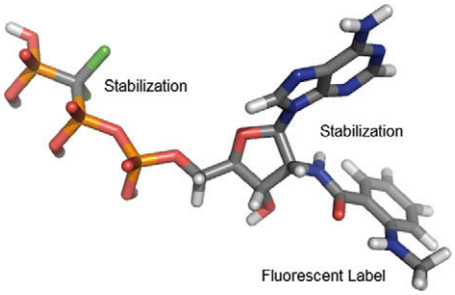

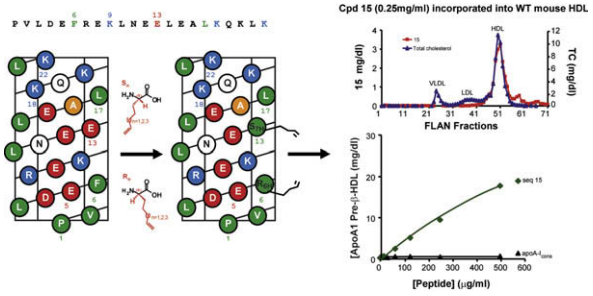

A serires of novel 2′3′-dideoxy-2′,3′-diethanethioribonucleosides with triazole ring were prepared and their antitumour activity was evaluated.

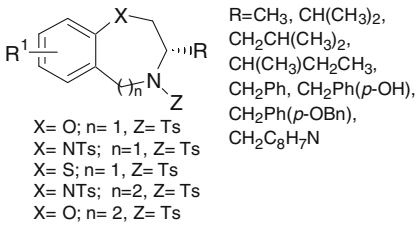

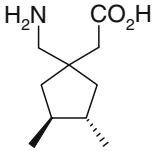

(21)
IC_{50}=22nM

A range of 3,4-disubstituted gababutins were synthesised and, of these, the stand-out compound was (**21**). This compound was profiled in in vivo models of pain and anxiety.

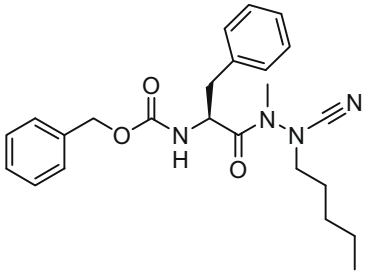

P. falciparum Dd2 IC_{50} = 2.1 μM

Falcipain-2 IC_{50} = 310 nM

Falcipain-3 IC_{50} = 110 nM

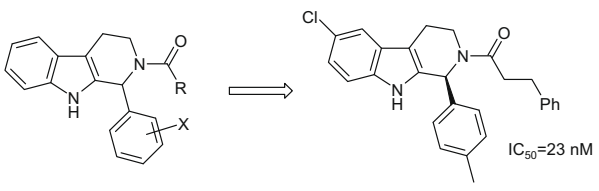

The identification and optimization of a series of substituted tetrahydro-β-carbolines with potent activity against human papillomavirus is described. Structure–activity studies focused on the substitution pattern and chirality of the β-carboline ring system are discussed. Optimization of these parameters led to compounds with antiviral activities in the low nanomolar range.

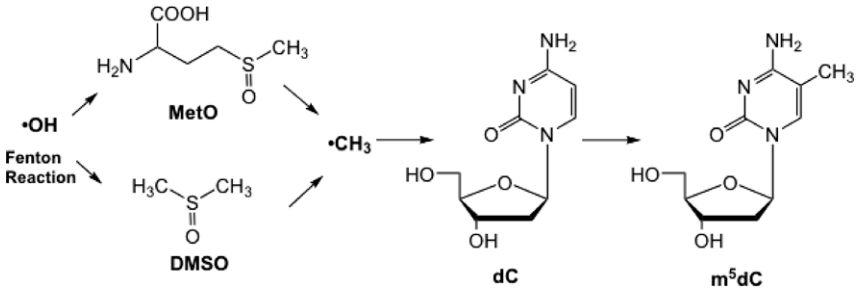

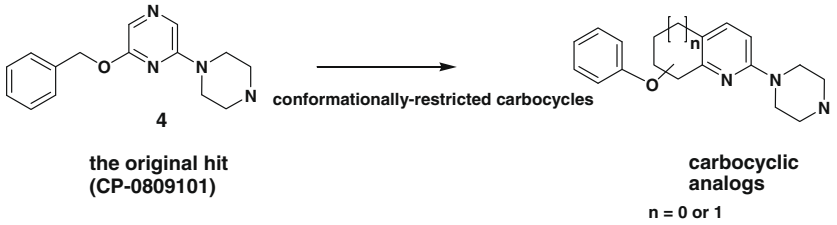

A series of novel conformationally-restricted 5HT2c receptor agonists with 2-piperazin-azaindane scaffold were designed. Orally-active compounds were identified with excellent functional selectivity against 5HT2a and 5HT2b receptors and with excellent 2c potency.

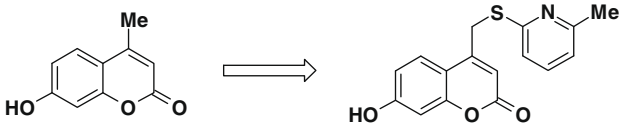

1
IC_{50} = 1.0 μM

4p
IC_{50} = 0.0015 μM

Compound **4p** was identified as a potent selective inhibitor of 17β-HSD3 resulting in the discovery of a novel lead series for further optimization.

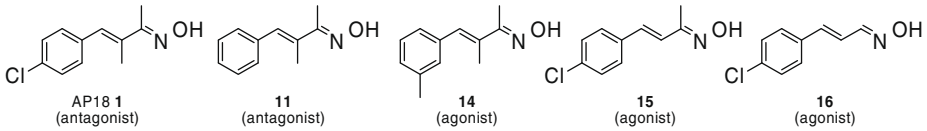

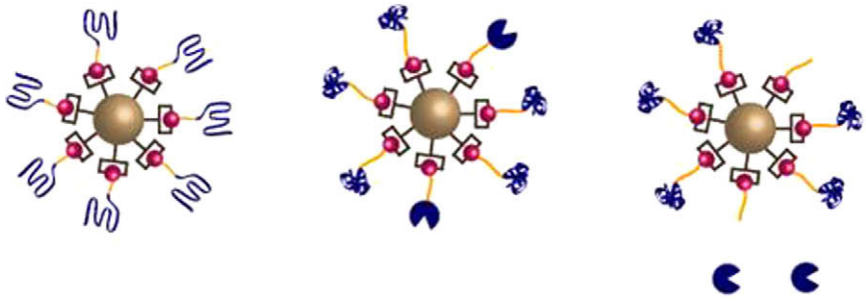

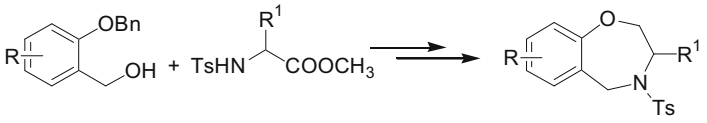

The active compound based on amino acid based benzoxazepine could cause significant reduction in tumor volume of MCF-7 xenograft tumor in nude mice model and the activity was comparable to that of tamoxifen citrate at 16 mg kg^{-1} dose at 30 days of treatment.

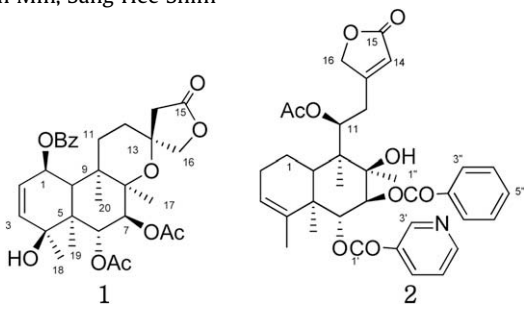

Two novel neo-clerodane diterpenoids, barbatellarine A (**1**) and B (**2**), were isolated from *Scutellaria barbata*, together with the known compound, scutebarbatine F (**3**). Compound **2** exhibited weak cytotoxic activity against HL-60 cell lines.

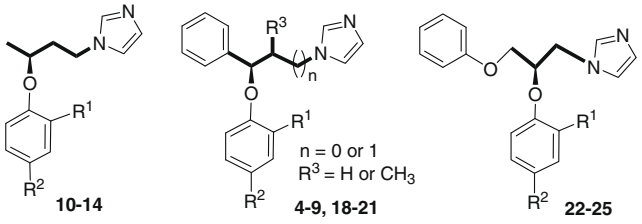

A series of aryloxy alkyl and aryloxy aryl alkyl imidazoles were synthesized and evaluated both in vitro and in vivo against *Leishmania donovani*. All the 19 compounds displayed very promising in vitro inhibition of 94–100% against promastigotes while two compounds showed medium in vivo inhibition of 58% and 60%.

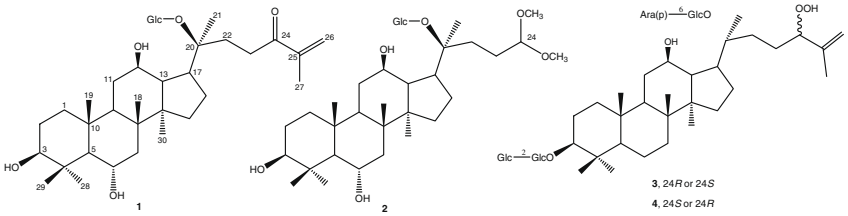

Six dammarane-type saponins, including three new floralginsenosides Ta–Tc (**1**–**3**), one first isolated from nature, floralginsenoside Td (**4**), along with two known ones, ginsenosides F_1 (**5**) and F_5 (**6**), were isolated from the flower buds of *Panax ginseng*. Compounds **1**, **5**, and **6** showed inhibitory effects on the growth of HL-60 cells with IC_{50} of 36.3, 23.2, and 62.4 μM, respectively.

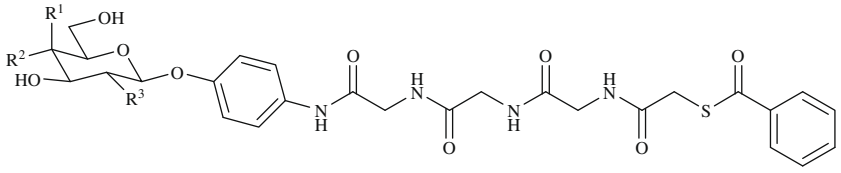

7 R^1=H; R^2=OH; R^3=OH
8 R^1=OH; R^2= H; R^3=OH
9 R^1=H; R^2=OH; R^3=NHAc

Synthesis of carbohydrate derivatives with mercaptoacetyltriglycine (MAG_3), radiolabeling with technetium-99m and biodistribution studies in mice.

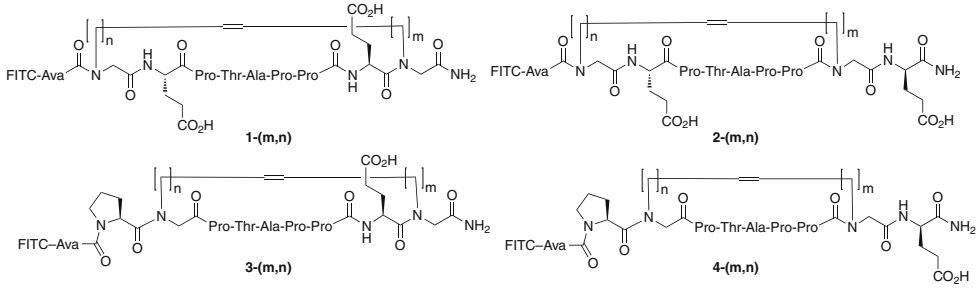

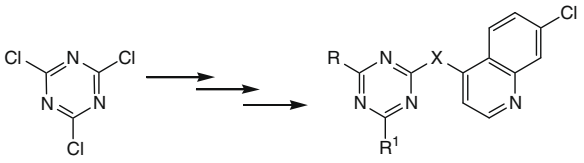

P. falciparum (D6 Clone); IC_{50} = 0.21 - 3.17 μM
P. falciparum (W2 Clone); IC_{50} = 0.22 - 3.53 μM

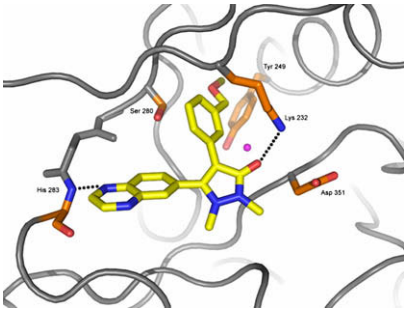

Interruption of TGFβ signaling through inhibition of the TGFβR1 kinase domain may prove to have beneficial effect in both fibrotic and oncological diseases. Herein we describe the SAR of a novel series of TGFβR1 kinase inhibitors containing a pyrazolone core. Most TGFβR1 kinase inhibitors described to date contain a core five-membered ring bearing N as H-bond acceptor. Described herein is a novel strategy to replace the core structure with pyrazolone ring, in which the carbonyl group is designed as an H-bond acceptor to interact with catalytic Lys 232.

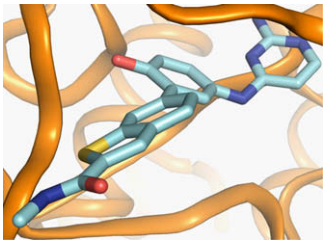

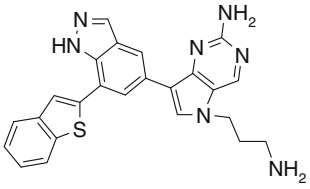

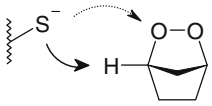

The reaction pathways of deprotonation versus nucleophilic substitution involving mPGES-2 enzyme catalysis were investigated by ab initio molecular orbital theory calculations for the reaction of methylthiolate with the endoperoxide core of PGH_2 and by the combined quantum mechanical molecular mechanical methods. The calculations showed that deprotonation mechanism is energetically more favorable than the nucleophilic substitution pathway.

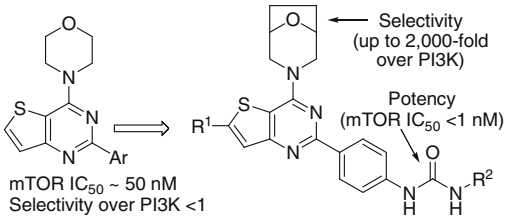

Introduction of bridged morpholine and ureidophenyl on moderately potent thienopyrimidine dual PI3K/mTOR inhibitors led to excellent mTOR potency and selectivity over PI3K.

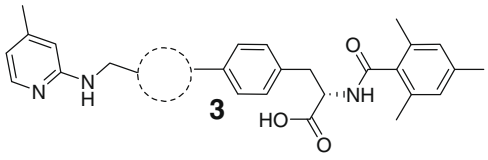

Combining structural features of integrin α5β1 antagonists leads to the generic structure **3**. The compounds expressing high integrin α5β1 binding affinities, low systemic clearances and long terminal half-lifes in male Wistar rat. Promising oral bioavailabilities were also observed for these compounds.

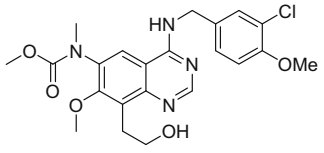

Property-based design of potent and selective PDE5 inhibitor is described.

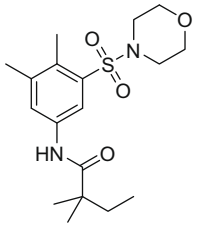

The discovery and SAR studies of a series of xylene sulfonamides as CB_2 selective agonists are reported.

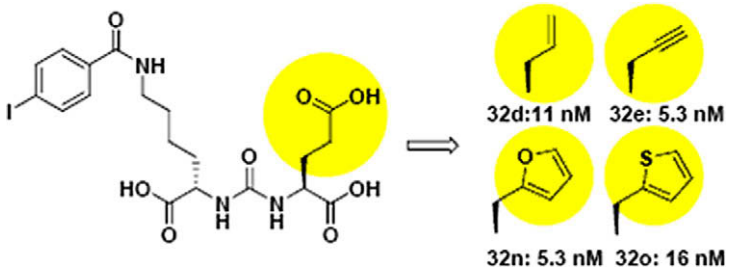

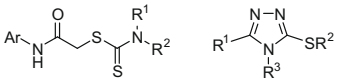

Two classes of compounds, thiocarbamates **1** and triazoles **2**, have been identified as HIV RT RNase H inhibitors using a novel FRET-based HTS assay. The potent analogs in each series exhibited selectivity and were active in cell-based assays. In addition, saturable, 1:1 stoichiometric binding to target was established and time of addition studies were consistent with inhibition of RT-mediated HIV replication.

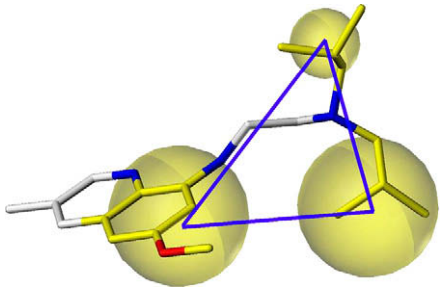

1-((Substituted)methyl)quinoxaline-2,3(1*H*,4*H*)-dione (**2a–e**) and 1-((substituted)acryloyl)quinoxaline-2,3(1*H*,4*H*)-dione (**4a–c**) were synthesized from quinoxaline-2,3(1*H*,4*H*)-dione **1** and evaluated for their antimicrobial activities. Results of the antitubercular screening against *Mycobacterium tuberculosis* $H_{37}Rv$ showed that the compounds **2b, 3,** and **4a** were the most effective, with minimum inhibitory concentrations of 8.012, 8.561, and 8.928 μg/ml, respectively. All the compounds exhibited significant antibacterial and considerable antifungal activities.

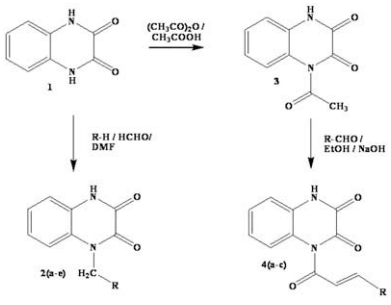

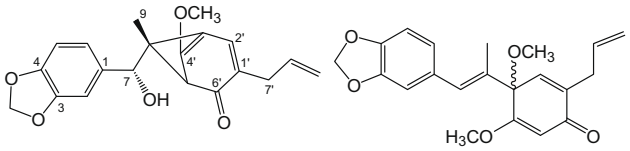

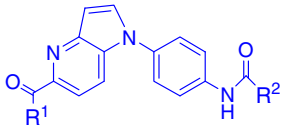

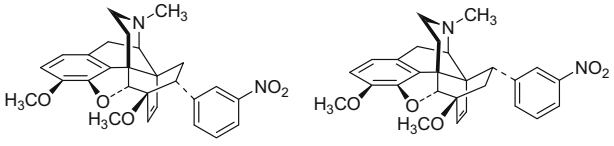

OTHER CONTENTS

*Corresponding author
Supplementary data available via ScienceDirect

COVER

Overlay of high resolution co-crystal structures of *R*-**22**-ADP (cyan) and **1**-ADP (green) bound in an allosteric binding site of the mitotic kinesin KSP. [Roecker, A. J.; Coleman, P. J.; Mercer, S. P.; Schreier, J. D.; Buser, C. A.; Walsh, E. S.; Hamilton, K.; Lobell, R. B.; Tao, W.; Diehl, R. E.; South, V. J.; Davide, J. P.; Kohl, N. E.; Yan, Y.; Kuo, L. C.; Li, C.; Fernandez-Metzler, C.; Mahan, E. A.; Prueksaritanont, T.; Hartman, G. D. *Bioorg. Med. Chem. Lett.* **2007**, *17*, 5677.]

Indexed/Abstracted in: Beilstein, Biochemistry & Biophysics Citation Index, CANCERLIT, Chemical Abstracts, Chemistry Citation Index, Current Awareness in Biological Sciences/BIOBASE, Current Contents: Life Sciences, EMBASE/Excerpta Medica, MEDLINE, PASCAL, Research Alert, Science Citation Index, SciSearch, TOXFILE. Also covered in the abstract and citation database SCOPUS®. Full text available on ScienceDirect®

ELSEVIER

ISSN 0960-894X